AGU ADVANCING EARTH AND SPACE SCIENCES

Geophysical Research Letters

RESEARCH LETTER
10.1029/2026GL125110

Key Points:
- Shock nonstationarity leads to localized structures with intense magnetic curvature at the shock foot
- Charge separation occurs in these structures and generates large-amplitude bipolar electric fields
- These structures pick up and accelerate thermal electrons, producing spiky bursts of electron beams in the upstream region

Supporting Information:
Supporting Information may be found in the online version of this article.

Correspondence to:
Q. Lu,
qmlu@ustc.edu.cn

Citation:
Guo, A., Lu, Q., Lu, S., Yao, S., & Gao, X. (2026). Spiky bursts of energetic electron beams upstream of nonstationary quasi-perpendicular shocks. *Geophysical Research Letters*, *53*, e2026GL125110. https://doi.org/10.1029/2026GL125110

Received 17 JUN 2026
Accepted 4 AUG 2026

Spiky Bursts of Energetic Electron Beams Upstream of Nonstationary Quasi-Perpendicular Shocks

Ao Guo[1,2], Quanming Lu[1,2], San Lu[1,2], Shutao Yao[3], and Xinliang Gao[1,2]

[1]Deep Space Exploration Laboratory, School of Earth and Space Sciences, University of Science and Technology of China, Hefei, China, [2]Collaborative Innovation Center of Astronautical Science and Technology, Harbin, China, [3]Shandong Provincial Key Laboratory of Optical Astronomy and Solar-Terrestrial Environment, Institute of Space Sciences, Shandong University, Weihai, China

Abstract Energetic electron beams play a crucial role in collisionless shocks by driving upstream plasma waves and providing seed populations for diffusive shock acceleration. However, the processes responsible for their generation at quasi-perpendicular shocks remain poorly understood. Using two-dimensional fully kinetic particle-in-cell simulations, we identify a new mechanism for generating electron beams at the leading edge of the shock foot. During shock reformation, reflected ions induce strong magnetic field curvature, causing ions and electrons to decouple dynamically. The resulting localized net charge separation generates large-amplitude bipolar electric fields, which efficiently pick up and accelerate upstream electrons. We therefore refer to this novel mechanism as Reformation-driven Electron Pickup Acceleration (REPA), which generates intense and spatially localized bursts of energetic electron beams. This process exhibits strong agreement with high-resolution observations upstream of Earth's bow shock, and provides an unexpected acceleration pathway for thermal electrons.

Plain Language Summary Collisionless shocks, such as Earth's bow shock, can accelerate electrons and produce beams of energetic electrons ahead of the shock. These beams are important because they can generate plasma waves and radio emissions in space. However, how these energetic electron beams form has remained unclear. Using advanced numerical simulations, we show that the shock front is not steady but repeatedly reforms. During this process, localized electric field structures appear at the edge of the shock. These structures act like moving mirrors that reflect and energize incoming electrons, creating spiky bursts of energetic beams. The simulated energy increase of these beams matches recent spacecraft observations. Our results show that the varying nature of shock fronts plays a key role in electron acceleration.

1. Introduction

Collisionless shocks are fundamental phenomena occurring throughout space, astrophysical, and laboratory plasmas (Jones & Ellison, 1991; Russell et al., 1982; Tang et al., 2025). They are widely recognized as efficient sites of particle acceleration and energy dissipation. Depending on the angle between the upstream magnetic field and the shock normal (θ_{Bn}), shocks are classified as quasi-parallel shocks ($\theta_{Bn} < 45°$) and quasi-perpendicular shocks ($\theta_{Bn} > 45°$) (Bale et al., 2005; Balogh & Treumann, 2013; Burgess et al., 2005).

Among the various plasma populations interacting with shocks, energetic electron beams propagating into the upstream region are of paramount importance. These field-aligned electron beams carry substantial free energy capable of exciting secondary plasma waves (Bale et al., 1999; Gurnett et al., 1979; Pulupa et al., 2010; Williams et al., 2005), which can subsequently undergo nonlinear conversion into solar radio bursts (Bale et al., 1999; Che et al., 2017; Holman & Pesses, 1983; Jebaraj et al., 2021; Maloney & Gallagher, 2011; Melrose, 1980, 2017; Morosan et al., 2019). Furthermore, understanding the origin of these electron beams is crucial for solving the long-standing "injection problem" in cosmic ray physics, as they provide the non-thermal seed population required for Diffusive Shock Acceleration (DSA) (Bell, 1978; Drury, 1983; Fermi, 1954).

Over the past few decades, several theoretical models have been established to explain electron beam generation at quasi-perpendicular shocks. At high-Mach-number shocks, electrons are accelerated through shock surfing acceleration associated with electrostatic waves upstream of the shock front. (Amano & Hoshino, 2007, 2008; Hoshino & Shimada, 2002; Matsumoto et al., 2012, 2013, 2017). Another long-standing mechanism is shock drift acceleration (SDA), in which electrons gain energy from the motional electric field while drifting because of the magnetic gradient at the shock front (Amano et al., 2022; Wu, 1984). Furthermore, while undergoing SDA, electrons may experience stochastic pitch angle scattering by high-frequency waves in the shock transition (Amano et al., 2020; Katou & Amano, 2019), which can greatly enhance their energy gain. This process is termed stochastic shock drift acceleration (SSDA). Some three-dimensional (3D) shock simulations also showed that electron acceleration can be modulated by ion-scale processes at the shock front (Trotta & Burgess, 2019).

Despite these theoretical advancements, a critical problem remains unresolved: how intense electron beams can be efficiently generated directly from the ambient thermal plasma under low-to-moderate Mach number conditions, where traditional mechanisms face severe physical limitations. For SSA, microscopic instabilities such as the Buneman instability exhibit remarkably high relative drift thresholds, making them difficult to excite at heliospheric shocks (Matsumoto et al., 2012). On the other hand, in SDA, only electrons with pitch angles outside the shock loss cone can be reflected upstream (Holman & Pesses, 1983). As a result, the fraction of thermal electrons that can enter the SDA process is typically small at heliospheric shocks, resulting in a relatively tenuous, spatially diffuse electron beam population. Consequently, the exact physical process that bridges the gap between thermal background electrons and the intense upstream electron beams frequently detected by high-resolution spacecraft observations at Earth's bow shock (Lindberg et al., 2023; Liu et al., 2025) remains poorly understood.

In this manuscript, we address this unresolved issue by exploring the role of shock nonstationarity in driving localized electron acceleration. Using two-dimensional (2D) fully kinetic particle-in-cell (PIC) simulations of an oblique quasi-perpendicular shock with moderate Mach number ($\theta_{\mathrm{Bn}} = 60°, M_A \approx 8.5$), we identify a novel mechanism operating at the leading edge of the shock foot. We demonstrate that during the cyclic process of shock reformation, the local accumulation of reflected ions induces an intense, localized bending of the magnetic field lines. This structural nonstationarity induces charge separation between magnetized electrons and unmagnetized ions, which self-consistently generates large-amplitude bipolar parallel electric fields. These electric fields act as highly efficient local injectors that directly pick up and accelerate background thermal electrons, producing the spiky bursts of field-aligned electron beams observed upstream. We refer to this mechanism as Reformation-driven Electron Pickup Acceleration (REPA), which provides a direct kinetic link between shock nonstationarity and upstream electron beams.

2. Simulation and Observational Data

The simulation is carried out by using an open-source relativistic full PIC code called SMILEI (Derouillat et al., 2018). A 2D simulation box with a size $L_x = 56.32\, d_{i0}$, $L_y = 10.24\, d_{i0}$ is employed in the $x - y$ plane, where $d_{i0} = c/\omega_{pi0}$ is the ion inertial length in the upstream region. For the particles, an open boundary is employed at $x = 0$, while a reflecting boundary is employed at $x = L_x$. For the electromagnetic fields, both the left and right boundaries are treated as conducting boundaries. Periodic boundary conditions are employed for both particles and fields in y direction. The particles are initially set to follow an isotropic drifting Maxwellian distribution with a bulk velocity of $\boldsymbol{V}_{\mathrm{in}} = 6V_{A0}\hat{\boldsymbol{x}}$ (where V_{A0} is the Alfvén speed in the upstream plasma). Particles with the same velocity distribution are also continuously injected from the left boundary. The shock propagates leftward with an average speed of approximately $-2.5V_{A0}$, corresponding to an Alfvén Mach number (M_A) of about 8.5. The ratio of the upstream Alfvén speed to the speed of light is set to $V_{A0}/c = 0.01$. Initially, a uniform background magnetic field is set with a large out-of-plane component: $\boldsymbol{B}_0 = B_0 \cos\theta_{\mathrm{Bn}}\hat{\boldsymbol{x}} + B_0 \sin\theta_{\mathrm{Bn}}\hat{\boldsymbol{z}}$, where $\theta_{\mathrm{Bn}} = 60°$ is the shock normal angle. The temperatures are set such that the ion plasma beta ($\beta_i = \frac{n_0 T_i}{B_0^2/2\mu_0}$) is 0.1 and the electron plasma beta (β_e) is 0.2. We adopt the proton-to-electron mass ratio of $m_p/m_e = 100$. The spatial resolution is $\Delta x = \Delta y = 0.01\, d_{i0}$, with each cell containing 100 computational particles. The time step of the simulation is set as $5 \times 10^{-5}\, \Omega_{i0}^{-1}$, where $\Omega_{i0} = \frac{eB_0}{m_i}$ is the ion gyro-frequency.

For comparison with spacecraft observations, we use a crossing of Earth's bow shock on 10 January 2020 around 16:21:15 UTC by the magnetospheric multiscale (MMS) spacecraft. The shock normal is determined using a mixed magnetic and velocity coplanarity method (Abraham-Shrauner, 1972), while upstream and downstream states are averaged over 16:20:28–16:20:40 UTC and 16:21:30–16:22:00 UTC, respectively. This yields $n = [-0.85, -0.47, 0.23]$ in GSE coordinates. The corresponding shock normal angle is $\theta_{\mathrm{Bn}} = 79°$, and the upstream Alfvén Mach number is $M_A \sim 8.3$, which are close to the simulated shock parameters. To enable a direct comparison with the simulation, ion and electron velocity distributions are transformed into the normal incident frame (NIF), which moves at $[-185.99, 206.80, -70.47]$ km/s relative to GSE.

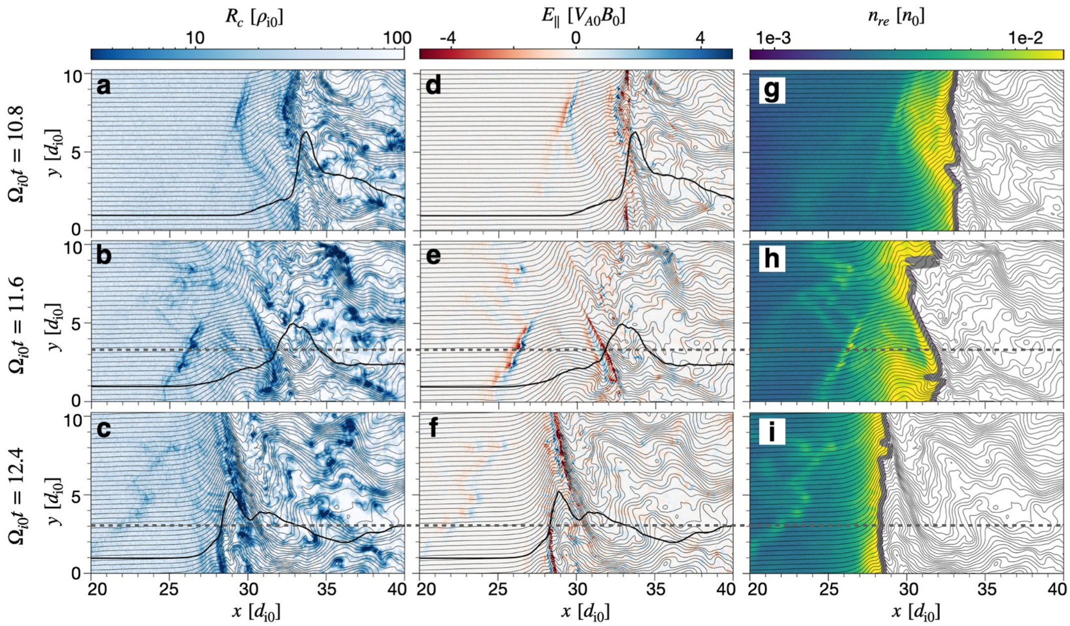

Figure 1. The shock structure at $\Omega_{i0}t = 10.8, 11.6,$ and 12.4. Gray contours in all figures represent the magnetic field lines. The magnetic field strength averaged over y axis ($\overline{B}/B_0$) is also plotted by the black lines in (a–f). (a–c) Colors represent the curvature radius of the magnetic field lines ($R_c = \frac{1}{|(\boldsymbol{b} \cdot \nabla)\boldsymbol{b}|}$). (d–f) Colors represent the electric field component parallel to the magnetic field ($E_\parallel$). (g–i) Colors represent the number density of the shock-reflected electrons (n_{re}). These electrons are defined by electrons with pitch angles larger than 100° upstream of the shock front. The gray lines mark the identified shock front.

3. Results

Figure 1 shows the structure of the shock after it is fully developed and separated from the right boundary of the simulation domain. A movie version of this figure showing the evolution of shock structure from $\Omega_{i0}t = 10.0$ to 12.7 is also available in Movie S1. The shock exhibits a quasi-periodic reformation process primarily driven by ion reflection at the shock front (Bale et al., 2005; Matsukiyo & Scholer, 2006). At $\Omega_{i0}t = 10.8$ (Figure 1a), the shock front is located at $x \approx 33.5\, d_{i0}$, about 23 d_{i0} away from the right boundary. A fraction of ions is reflected by the shock front, forming a gradual increase in magnetic field strength and plasma density ahead of the shock ramp, namely the shock foot. With the presence of the out-of-plane magnetic field B_z, shock-reflected ions predominantly gyrate in the $x - y$ plane, bending the in-plane magnetic field lines in the shock foot. Because the magnetic field strength along the shock front is spatially inhomogeneous, ion reflection occurs nonuniformly. Steeper ramp segments can reflect more ions and produce a more extended upstream foot.

This nonuniform ion reflection leads to spatiotemporally inhomogeneous shock reformation and promotes the formation of localized structures. The distorted magnetic field lines in the foot region introduce magnetic curvature at the boundary between the foot and the upstream plasma. A larger population of reflected ions within the shock foot leads to stronger bending of the magnetic field lines. At some localized regions with intensified ion reflection (e.g., $x \approx 29$–$30\, d_{i0}, y \approx 6$–$10 d_{i0}$ in Figure 1a), the curvature radius becomes comparable to the ion gyroradius ($R_c \sim \rho_{i0}$, where $R_c = \frac{1}{|(\boldsymbol{b} \cdot \nabla)\boldsymbol{b}|}$ is the curvature radius of magnetic field lines, and $\rho_{i0} = \frac{m_i V_{th,i}}{B_0 e}$ is the upstream ion gyroradius). Under these conditions, ion motion becomes nonadiabatic and decouples from the magnetic field, whereas electrons remain magnetized, resulting in charge separation and the generation of a bipolar parallel electric field (Figure 1d). This bipolar electric field structure forms at the upstream edge of the shock foot, and propagates in the $-x$ direction as the foot region expands (Figures 1b and 1e). It has a width of about 2 d_{i0}, which is significantly larger than those typical Debye-scale ESWs generated by Buneman or electron two-stream instabilities in high-Mach-number shock simulations (Amano & Hoshino, 2007, 2008; Hoshino & Shimada, 2002). At $\Omega_{i0}t = 11.6$, the bipolar electric field structure reaches its maximum amplitude (about 5 $V_{A0}B_0$), which is comparable to the electric field strength near the shock front (Figure 1e). At $\Omega_{i0}t = 12.4$, as the previous shock foot at $x \approx 29\, d_{i0}$ steepens and evolves into a new shock front, the new shock foot subsequently contracts back to $x \approx 27$–$28\, d_{i0}$. The amplitude of the former bipolar electric field weakens and the

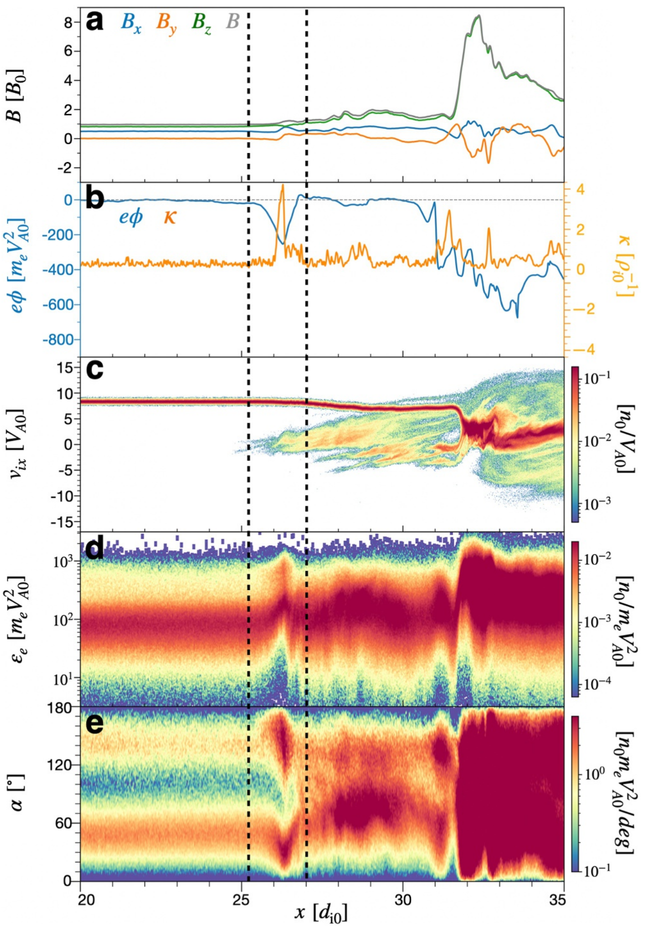

Figure 2. Profiles of physical quantities sampled at $\Omega_{i0}t = 11.6$ along the line $y = 3.3d_{i0}$ (dashed cut indicated in the second row of Figure 1). All quantities are transformed into the normal incident frame. (a) The three components of the magnetic field and its magnitude. (b) The electrostatic potential eϕ along the magnetic field line started at $y = 3.3d_{i0}$, and the magnetic field curvature $\kappa = |(b \cdot \nabla) b|$. (c) The ion velocity distribution in the x direction. (d) The electron energy distribution. (e) The electron energy flux as a function of pitch angle. Dashed lines mark out the position of the bipolar electric field structure.

associated magnetic curvature diminishes (Figures 1c and 1f). During the formation and propagation of the bipolar electric field structures, distinct electron beams are generated at their corresponding locations (Figures 1g–1i), where beam electrons are defined as upstream electrons with pitch angles exceeding 100°. These beam electrons remain clustered in the upstream region even after the bipolar electric field structures have weakened (Figure 1i). The generation process of these beam electrons will be discussed in Figure 4, which we refer to as REPA.

To further investigate the properties of this bipolar electric field structure, we present quantities along two representative cuts in Figures 2 and 3. Figure 2 is taken at the time when the structure reaches its maximum amplitude (dashed line in the second row of Figure 1), and Figures 3a–3e is taken at a later time when it gradually dissipates in the upstream region (dashed line in the third row of Figure 1). All quantities are transformed into the NIF, which is stationary relative to the shock front. At $\Omega_{i0}t = 11.6$, the bipolar parallel electric field is observed between $x \approx 25$–$27\,d_{i0}$. By integrating the electric field along magnetic field lines, we obtain the electrostatic potential at different locations (eϕ = e$\int_0^x E \cdot b ds$, where s is the distance along the magnetic field line). The center of the bipolar electric field structure corresponds to a potential drop of approximately $-300\,m_e V_{A0}^2$, while the cross-shock potential is about $-500\,m_e V_{A0}^2$ (Figure 2b). Notably, the electrostatic potential at the right boundary of the bipolar structure is slightly positive (Figure 2b, $x \approx 26.9\,d_{i0}$), indicating that electrons with relatively small parallel velocities can be picked up and trapped by the structure. The strong magnetic field curvature observed at the leading edge of the shock foot is primarily caused by magnetic field variations in the x and y directions (Figure 2a). The peak in magnetic field curvature coincides with the center of the bipolar electric field structure at $x \approx 26.2\,d_{i0}$, corresponding to the boundary between the shock foot and the upstream region. This location marks the furthest upstream extent reached by shock-reflected ions, where their velocity in the x direction approaches zero before they gyrate back toward the downstream region (Figure 2c).

Within this region, a significant enhancement of electron energy is evident (Figure 2d). The pitch-angle distribution of these energetic electrons is concentrated primarily between 120° and 180° (Figure 2e), whereas upstream electrons are mainly distributed between 10° and 70°. This means intense field-aligned electron beams are formed by REPA within the bipolar electric field structure. The maximum distance between the bipolar electric field and the shock front is controlled by the thickness of shock foot, which can be estimated by $\Delta L = \frac{0.68\,M_A V_{A0} m_p}{e B_0} \sin\theta_{\rm Bn}$ (Gosling & Thomsen, 1985; Livesey et al., 1984). This indicates that, as $\theta_{\rm Bn}$ increases, the electric field structure can propagate further upstream away from the shock. However, large $\theta_{\rm Bn}$ inherently constrains the accelerated electrons from propagating far into the upstream as the field lines are nearly parallel to the shock front. At $\Omega_{i0}t = 12.4$, the shock front has reformed and shifted to $x \approx 28.5\,d_{i0}$ (Figure 3a), and the ion velocity distribution exhibits the characteristic ring-like structure associated with shock reformation (Figure 3c) (Lotekar et al., 2025; Yang et al., 2020). Meanwhile, the previous bipolar electric field structure has propagated upstream to $x \approx 21$–$22.5\,d_{i0}$, where both the electric field amplitude and magnetic field curvature are substantially reduced (Figure 3b). The electrostatic potential at the right boundary of the structure also drops below zero ($x \approx 22.5\,d_{i0}$), indicating that no more upstream electrons are being picked up. However, energetic electron beams propagating antiparallel to the magnetic field remain clear (Figures 2d and 2e). The density of these electron beams is about 1% of the upstream electron density (Figure 1i), and their field-aligned relative drift to the upstream electrons is approximately $30V_{A0}$. This corresponds to ~7.5 upstream electron thermal speeds and an energy about 10 times that of the background electrons. One-dimensional projections are also provided only as auxiliary visualization in Figure S1.

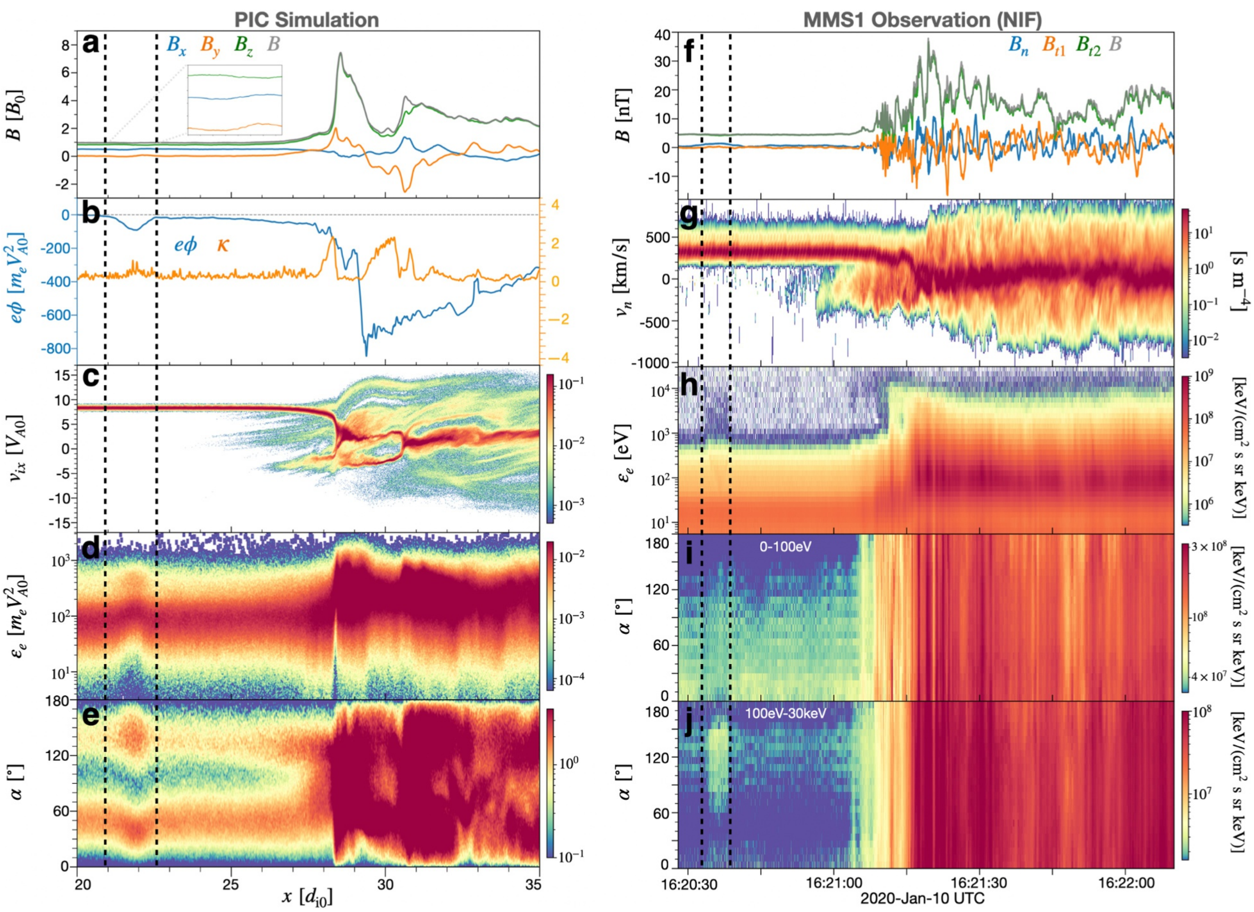

Figure 3. Direct comparison of spiky electron beams upstream of quasi-perpendicular shocks: PIC simulation (a–e) versus MMS1 observation (f–j). (a–e) Profiles of simulation quantities sampled at $\Omega_{i0}t = 12.4$ along the line $y = 3.0\,d_{i0}$ (dashed cut indicated in the third row of Figure 1), which are organized the same in Figure 2 (f–j) MMS1 measurements of a crossing of Earth's quasiperpendicular bow shock. All quantities are transformed into the NIF as described in Section 2. (f) The magnetic field. (g) Distribution of ion velocity along the shock normal (v_n). (h) The electron spectrum. (i–j) Electron pitch angle distribution in energy ranges of 0–100 eV and 100 eV-30 keV, respectively.

Spiky enhancements of energetic electron flux accompanied by field-aligned beams have been frequently detected by MMS spacecraft upstream of Earth's quasi-perpendicular bow shock (Lindberg et al., 2023; Liu et al., 2025). Here, we present a typical event (Figures 3f–3j) observed by MMS1 for a side-by-side comparison with the simulation results. We obtain an Alfvén Mach number (M_A) of about 8.3 and a shock-normal angle (θ_{Bn}) of approximately 79° for this event (Section 2), which are close to the shock parameters used in the simulation. As shown in Figure 3, the simulation reproduces the key observational signatures observed by MMS. There is a bending of the magnetic field line in N direction between the two dashed lines (Figure 3f). Crucially, the electron energy spectra and pitch angle distributions show excellent qualitative and quantitative agreement. In both MMS data and our simulation, there is: 1. A localized, spiky energy enhancement of $1 \sim 2$ orders of magnitude (Figures 3d and 3h); 2. A low-energy population of incoming electrons with pitch angles ranging from 0° to 60° in NIF (Figures 3e and 3i); 3. A high-energy population of beam electrons with pitch angles ranging from 120° to 180° in NIF (Figures 3e and 3j). This consistency between simulation and observation suggests REPA as a compelling explanation for bursts of electron beams upstream of Earth's bow shock.

The generation of these bursts of energetic electron beams through REPA is then analyzed by particle tracing. We present two different kinds of shock-reflected electrons in Figure 4. Figures 4a–4c show a representative electron reflected by the bipolar electric field structure. As this electron moves from the upstream region toward the edge of the shock foot, it encounters a bipolar electric field and undergoes REPA (Figure 4a). The reflection occurs precisely within the region with positive $E_\parallel$ inside the bipolar electric field structure shown in Figure 1a ($x \approx 30\,d_{i0}; y \approx 8.3\,d_{i0}$). While entering the structure, the electron's parallel velocity is rapidly modified by the

10.1029/2026GL125110

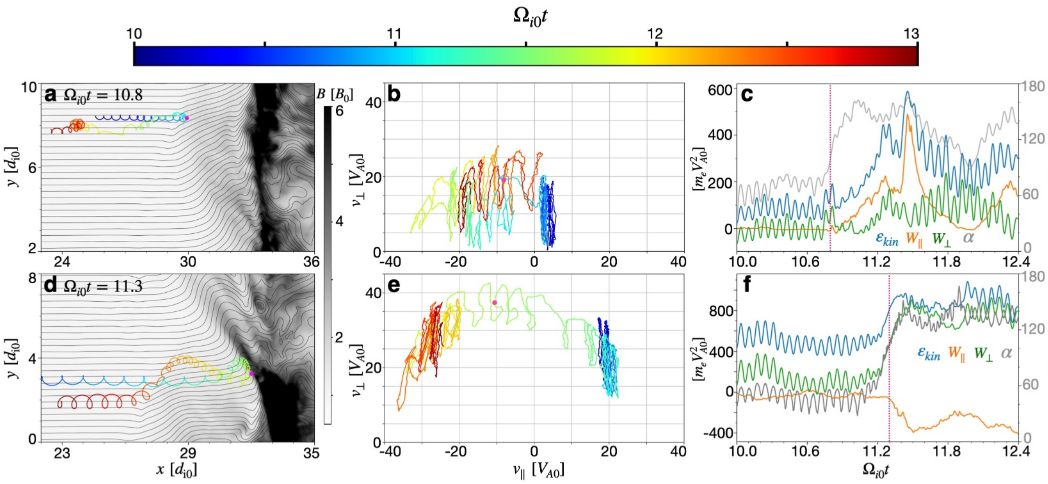

Figure 4. Trajectories of two representative shock-reflected electrons. (a–c) An electron reflected by the bipolar electric field structures in the shock foot, and (d–f) an electron energized via SDA. (a, d) The magenta dot marks the location where the electron reaches its maximum x (i.e., the reflection point). The colored curve shows the electron trajectory, with color indicating temporal progression. The grayscale background represents the magnetic-field strength B at the reflection time, and black curves denote magnetic field lines. (b, e) Temporal evolution of the electron velocity components parallel ($v_\parallel$) and perpendicular ($v_\perp$) to the magnetic field. The magenta dot indicates the reflection point. (c, f) Time evolution of the electron kinetic energy (ε_{kin}), pitch angle (α), and the work done by the parallel and perpendicular electric field components ($W_\parallel = \int_{t_0}^{t} E_\parallel v_\parallel dt$, and $W_\perp = \int_{t_0}^{t} E_\perp \cdot v_\perp dt$). The magenta dashed line marks the reflection time. All quantities are transformed into the shock-rest frame.

parallel electric field, causing it to reverse direction and move upstream (Figure 4b). During the reflection process, the electron's kinetic energy changes only slightly, whereas its pitch angle increases rapidly from $\sim 60°$ to values exceeding $140°$ (Figure 4c, $\Omega_{i0}t \approx 10.8$). After reflection, the electron becomes trapped between the bipolar electric fields and propagates upstream together with the structure. Variations in the electron velocity occur predominantly in the parallel direction (Figure 4b). As the electron bounces back and forth between the positive and negative $E_\parallel$ region in the structure, its energy exhibits noticeable fluctuations during $\Omega_{i0}t = 10.9$–12.4 (Figure 4c). The electron is accelerated to $\varepsilon_{\text{kin}} \approx 600\, m_e V_{A0}^2$ by $E_\parallel$ at $\Omega_{i0}t \approx 11.5$ and eventually settles at an energy of about $300\, m_e V_{A0}^2$ when the bipolar electric field diminishes. This overall energy gain is mainly from the electrostatic potential energy in the bipolar electric field structure, which corresponds to the maximum potential drop at its center ($\sim 300\, m_e V_{A0}^2$, Figure 2b).

In comparison, Figures 4d–4f present an electron that is energized by SDA at the shock front. This electron does not encounter the bipolar electric field structures while entering the shock foot. Instead, it is reflected in the region of strong magnetic field at the shock ramp (Figure 4d). While undergoing gradient-B drift along the shock front, the electron is accelerated by the upstream convection electric field ($\boldsymbol{E} = \boldsymbol{V} \times \boldsymbol{B}$), which means it gains energy mainly from $\boldsymbol{E}_\perp$ (Figure 4f, $\Omega_{i0}t = 11.2$–11.4). During this period, its pitch angle evolves concurrently from $\sim 50°$ to $\sim 140°$. The velocity evolution of this electron during reflection traces a characteristic arc-shaped trajectory in velocity space (Figure 4e), which is typical in SDA as it is an energy-conserving process in the de Hoffmann–Teller (HT) frame (de Hoffmann & Teller, 1950; Wu, 1984).

In order to enter SDA, electrons must possess sufficiently high initial energies and pitch angles larger than the shock loss-cone angle in the HT frame. For example, the SDA electron shown in Figure 4d has an initial energy of approximately $600\, m_e V_{A0}^2$, which is significantly higher than the mean energy of upstream electrons ($\sim 36\, m_e V_{A0}^2$). Upstream thermal electrons that can directly enter SDA are exceedingly rare. As a consequence, when no bipolar electric field structure is present upstream of the shock, the population of shock-reflected electrons is relatively tenuous, with a density of only $\sim 10^{-3}$ of the upstream electron density (Figure 1g). Unlike SDA, REPA substantially lowers the threshold required for electron reflection and acceleration. It has a pronounced impact on a much larger population of thermal electrons. As the bipolar electric field structures propagate upstream, they continuously pick up and accelerate electrons with relatively small parallel velocities. This process leads to a substantial enhancement of beam electrons within the structures. The density of electron beams within these structures is approximately an order of magnitude higher than that in the surrounding plasma (Figures 1h and 1i).

4. Discussion

The generation of bursty electron beams identified in this work differs fundamentally from steady-state acceleration scenarios traditionally invoked for quasi-perpendicular shocks. Instead of continuous energization, REPA is highly intermittent and localized, reflecting the intrinsically nonstationary nature of the shock front. Through localized large-amplitude electric fields, REPA efficiently accelerates thermal electrons that would otherwise fail the SDA reflection condition.

Electron beams are common in various plasma processes and were investigated in the context of magnetic reconnection over a decade ago (e.g., Chang et al., 2022; Che et al., 2009, 2010; Huang et al., 2014). Satellite observations upstream of Earth's bow shock have also found that electrons can be accelerated by localized electric field structures along the magnetic field, reaching an electron–ion relative drift speed exceeding the electron thermal speed. The secondary instabilities triggered by this beam can then lead to upstream electron heating (Chen et al., 2018). While heating efficiency is notable, it is limited at low Mach numbers (Che et al., 2013), because both Buneman and two-stream instabilities have high relative beam velocity thresholds $\sim 3v_{te}$ (Che, 2016). Here, we report an efficient electron acceleration process that generates intense electron beams with a relative drift velocity of about $7.5v_{te}$. It carries sufficient free energy to excite secondary instabilities and produce localized electron heating.

To save computational cost, a reduced ion-to-electron mass ratio was employed in our study. This may compress the separation between ion scales and electron scales, which in turn affects the scale of the charge separation electric field. However, the fundamental physics driving the charge separation remains unaltered as it is governed by macroscopic ion reflection. Also, a realistic mass ratio may allow electrons to be accelerated more rapidly by the electric field, thereby affecting the final velocity of the resulting electron beam. Under certain conditions, it may even overcome the threshold required for the generation of radio bursts, thereby producing electromagnetic emissions (Che et al., 2017, 2023). However, the present study only focuses on the generation mechanism of these electron beams. The subsequent heating or secondary instabilities induced by the beams might not be fully resolved because of the limitation of 2D geometry, as the out-of-plane magnetic field configuration suppresses field-aligned processes. Future 3D simulations are needed to quantify the beam dissipation and trapping efficiency, although the agreement with MMS observations suggests that the present 2D model captures the key properties of REPA.

5. Conclusions

In this work, we have identified a previously underappreciated mechanism for electron pre-acceleration at quasi-perpendicular collisionless shocks, which we term REPA. We show that shock nonstationarity leads to the generation of bursty energetic electron beams upstream of the shock. Shock reformation naturally produces localized electromagnetic micro-structures with strong magnetic curvature upstream of the shock front. These structures generate intense, transient parallel electric fields capable of rapidly accelerating electrons. The resulting upstream electron beams are highly intermittent and appear as spiky energetic bursts, reflecting the nonstationary nature of the shock. Our novel mechanism highlights the importance of shock nonstationarity in shaping electron acceleration, which is supported by MMS observations that show remarkable agreement with simulation results.

Conflict of Interest

The authors declare no conflicts of interest relevant to this study.

Availability Statement

The simulation was performed using the open-source particle-in-cell code SMILEI, which is available at https://smileipic.github.io/Smilei/. MMS data used for comparison in this study are publicly available from the MMS Science Data Center (https://lasp.colorado.edu/mms/sdc/public/). The MMS data processing, coordinate transformations, and pitch angle distribution calculations were performed using the open-source Python package pyrfu, which is available at https://github.com/louis-richard/irfu-python. The simulation data used to plot the figures in this article can be downloaded from "National Space Science Data Center, National Science and Technology Infrastructure of China" (Guo, 2026).

Acknowledgments

This work was supported by the National Natural Science Foundation of China (NSFC, Grants 425B2023 and 42230201). The numerical computations in this paper were done at the Supercomputing Center of University of Science and Technology of China. We acknowledge the MMS Fast Plasma Investigation (FPI) team for providing the high-quality plasma data used for comparison in this study. We thank the developers of the pyrfu analysis package for providing the open-source tools that facilitated the MMS spacecraft data analysis in this study. We acknowledge the MMS bow shock crossing database developed by Lalti et al. (2022), which greatly facilitated our event selection in this study.

References

Abraham-Shrauner, B. (1972). Determination of magnetohydrodynamic shock normals. *Journal of Geophysical Research (1896-1977)*, *77*(4), 736–739. https://doi.org/10.1029/JA077i004p00736

Amano, T., & Hoshino, M. (2007). Electron injection at high mach number quasi-perpendicular shocks: Surfing and drift acceleration. *The Astrophysical Journal*, *661*(1), 190–202. https://doi.org/10.1086/513599

Amano, T., & Hoshino, M. (2008). Electron shock surfing acceleration in multidimensions: Two-dimensional particle-in-cell simulation of collisionless perpendicular shock. *The Astrophysical Journal*, *690*(1), 244–251. https://doi.org/10.1088/0004-637X/690/1/244

Amano, T., Katou, T., Kitamura, N., Oka, M., Matsumoto, Y., Hoshino, M., et al. (2020). Observational evidence for stochastic shock drift acceleration of electrons at the earth's bow shock. *Physical Review Letters*, *124*(6), 065101. https://doi.org/10.1103/PhysRevLett.124.065101

Amano, T., Matsumoto, Y., Bohdan, A., Kobzar, O., Matsukiyo, S., Oka, M., et al. (2022). Nonthermal electron acceleration at collisionless quasi-perpendicular shocks. *Reviews of Modern Plasma Physics*, *6*(1), 29. https://doi.org/10.1007/s41614-022-00093-1

Bale, S. D., Balikhin, M. A., Horbury, T. S., Krasnoselskikh, V. V., Kucharek, H., Möbius, E., et al. (2005). Quasi-perpendicular shock structure and processes. *Space Science Reviews*, *118*(1–4), 161–203. https://doi.org/10.1007/s11214-005-3827-0

Bale, S. D., Reiner, M. J., Bougeret, J.-L., Kaiser, M. L., Krucker, S., Larson, D. E., & Lin, R. P. (1999). The source region of an interplanetary type II radio burst. *Geophysical Research Letters*, *26*(11), 1573–1576. https://doi.org/10.1029/1999GL900293

Balogh, A., & Treumann, R. A. (2013). Physics of collisionless shocks: Space plasma shock waves. *Physics of Collisionless Shocks: Space Plasma Shock Waves*, *12*. https://doi.org/10.1007/978-1-4614-6099-2

Bell, A. R. (1978). The acceleration of cosmic rays in shock fronts - I. *Monthly Notices of the Royal Astronomical Society*, *182*(2), 147–156. https://doi.org/10.1093/mnras/182.2.147

Burgess, D., Lucek, E. A., Scholer, M., Bale, S. D., Balikhin, M. A., Balogh, A., et al. (2005). Quasi-parallel shock structure and processes. *Space Science Reviews*, *118*(1–4), 205–222. https://doi.org/10.1007/s11214-005-3832-3

Chang, C., Huang, K., Lu, Q., Lu, S., Yu, X., Wang, R., et al. (2022). Electrostatic solitary waves and electron-beam instabilities in the separatrix region of magnetic reconnection. *The Astrophysical Journal*, *933*(1), 67. https://doi.org/10.3847/1538-4357/ac738d

Che, H. (2016). Electron two-stream instability and its application in solar and heliophysics. *Modern Physics Letters A*, *31*(19), 1630018. https://doi.org/10.1142/S0217732316300184

Che, H., Benz, A. O., & Zank, G. P. (2023). Particle-in-cell simulations – Ion beam instabilities and the generation of alfvén and whistler waves in low β plasma. *Monthly Notices of the Royal Astronomical Society*, *526*(2), 2110–2117. https://doi.org/10.1093/mnras/stad2897

Che, H., Drake, J. F., Swisdak, M., & Goldstein, M. L. (2013). The adiabatic phase mixing and heating of electrons in Buneman turbulence. *Physics of Plasmas*, *20*(6), 061205. https://doi.org/10.1063/1.4811137

Che, H., Drake, J. F., Swisdak, M., & Yoon, P. H. (2009). Nonlinear development of streaming instabilities in strongly magnetized plasma. *Physical Review Letters*, *102*(14), 145004. https://doi.org/10.1103/PhysRevLett.102.145004

Che, H., Drake, J. F., Swisdak, M., & Yoon, P. H. (2010). Electron holes and heating in the reconnection dissipation region. *Geophysical Research Letters*, *37*(11), 2010GL043608. https://doi.org/10.1029/2010GL043608

Che, H., Goldstein, M. L., Diamond, P. H., & Sagdeev, R. Z. (2017). How electron two-stream instability drives cyclic langmuir collapse and continuous coherent emission. *Proceedings of the National Academy of Sciences*, *114*(7), 1502–1507. https://doi.org/10.1073/pnas.1614055114

Chen, L.-J., Wang, S., Wilson, L. B., Schwartz, S., Bessho, N., Moore, T., et al. (2018). Electron bulk acceleration and thermalization at earth's quasiperpendicular bow shock. *Physical Review Letters*, *120*(22), 225101. https://doi.org/10.1103/PhysRevLett.120.225101

de Hoffmann, F., & Teller, E. (1950). Magneto-hydrodynamic shocks. *Physical Review*, *80*(4), 692–703. https://doi.org/10.1103/PhysRev.80.692

Derouillat, J., Beck, A., Pérez, F., Vinci, T., Chiaramello, M., Grassi, A., et al. (2018). Smilei: A collaborative, open-source, multi-purpose particle-in-cell code for plasma simulation. *Computer Physics Communications*, *222*, 351–373. https://doi.org/10.1016/j.cpc.2017.09.024

Drury, L. O. (1983). Review article: An introduction to the theory of diffusive shock acceleration of energetic particles in tenuous plasmas. *Reports on Progress in Physics*, *46*(8), 973–1027. https://doi.org/10.1088/0034-4885/46/8/002

Fermi, E. (1954). Galactic magnetic fields and the origin of cosmic radiation. *The Astrophysical Journal*, *119*, 1. https://doi.org/10.1086/145789

Gosling, J. T., & Thomsen, M. F. (1985). Specularly reflected ions, shock foot thicknesses, and shock velocity determinations in space. *Journal of Geophysical Research*, *90*(A10), 9893–9896. https://doi.org/10.1029/JA090iA10p09893

Guo, A. (2026). Data for "Spiky Bursts of Energetic Electron Beams Upstream of Nonstationary Quasi-Perpendicular Shocks"Data for "Spiky Bursts of Energetic Electron Beams Upstream of Nonstationary Quasi-Perpendicular Shocks" (version V2). *Science Data Bank*. [Dataset]. https://doi.org/10.57760/SCIENCEDB.27188

Gurnett, D. A., Neubauer, F. M., & Schwenn, R. (1979). Plasma wave turbulence associated with an interplanetary shock. *Journal of Geophysical Research*, *84*(A2), 541–552. https://doi.org/10.1029/JA084iA02p00541

Holman, G. D., & Pesses, M. E. (1983). Solar type II radio emission and the shock drift acceleration of electrons. *The Astrophysical Journal*, *267*, 837. https://doi.org/10.1086/160918

Hoshino, M., & Shimada, N. (2002). Nonthermal electrons at high mach number shocks: Electron shock surfing acceleration. *The Astrophysical Journal*, *572*(2), 880–887. https://doi.org/10.1086/340454

Huang, C., Lu, Q., Wang, P., Wu, M., & Wang, S. (2014). Characteristics of electron holes generated in the separatrix region during antiparallel magnetic reconnection. *Journal of Geophysical Research: Space Physics*, *119*(8), 6445–6454. https://doi.org/10.1002/2014JA019991

Jebaraj, I. C., Kouloumvakos, A., Magdalenic, J., Rouillard, A. P., Mann, G., Krupar, V., & Poedts, S. (2021). Generation of interplanetary type II radio emission. *Astronomy and Astrophysics*, *654*, A64. https://doi.org/10.1051/0004-6361/202141695

Jones, F. C., & Ellison, D. C. (1991). The plasma physics of shock acceleration. *Space Science Reviews*, *58*(1), 259–346. https://doi.org/10.1007/BF01206003

Katou, T., & Amano, T. (2019). Theory of stochastic shock drift acceleration for electrons in the shock transition region. *The Astrophysical Journal*, *874*(2), 119. https://doi.org/10.3847/1538-4357/ab0d8a

Lalti, A., Khotyaintsev, Y. V., Dimmock, A. P., Johlander, A., Graham, D. B., & Olshevsky, V. (2022). A database of MMS bow shock crossings compiled using machine learning. *Journal of Geophysical Research: Space Physics*, *127*(8), e2022JA030454. https://doi.org/10.1029/2022JA030454

Lindberg, M., Vaivads, A., Raptis, S., & Karlsson, T. (2023). MMS observation of two-step electron acceleration at earth's bow shock. *Geophysical Research Letters*, *50*(16), e2023GL104714. https://doi.org/10.1029/2023GL104714

Liu, Y. Y., Cao, J. B., Liu, C. M., Song, Y. T., & Hu, D. K. (2025). Electron acceleration by multiple fast fermi reflections at earth's bow shock. *The Astrophysical Journal*, *979*(2), 179. https://doi.org/10.3847/1538-4357/ada5f0

Livesey, W. A., Russell, C. T., & Kennel, C. F. (1984). A comparison of specularly reflected gyrating ion orbits with observed shock foot thicknesses. *Journal of Geophysical Research*, *89*(A8), 6824–6828. https://doi.org/10.1029/JA089iA08p06824

Lotekar, A., Khotyaintsev, Y. V., Graham, D. B., Dimmock, A., Johlander, A., & Lalti, A. (2025). Occurrence of non-stationarity at earth's quasi-perpendicular bow shock. *Geophysical Research Letters*, *52*(17), e2025GL116121. https://doi.org/10.1029/2025GL116121

Maloney, S. A., & Gallagher, P. T. (2011). STEREO direct imaging of a coronal mass ejection-driven shock to 0.5 AU. *The Astrophysical Journal*, *736*(1), L5. https://doi.org/10.1088/2041-8205/736/1/L5

Matsukiyo, S., & Scholer, M. (2006). On reformation of quasi-perpendicular collisionless shocks. *Advances in Space Research*, *38*(1), 57–63. https://doi.org/10.1016/j.asr.2004.08.012

Matsumoto, Y., Amano, T., & Hoshino, M. (2012). Electron accelerations at high mach number shocks: Two-dimensional particle-in-cell simulations in various parameter regimes. *The Astrophysical Journal*, *755*(2), 109. https://doi.org/10.1088/0004-637X/755/2/109

Matsumoto, Y., Amano, T., & Hoshino, M. (2013). Electron acceleration in a nonrelativistic shock with very high Alfvén Mach number. *Physical Review Letters*, *111*(21), 215003. https://doi.org/10.1103/physrevlett.111.215003

Matsumoto, Y., Amano, T., Kato, T. N., & Hoshino, M. (2017). Electron surfing and drift accelerations in a Weibel-dominated high-Mach-number shock. *Physical Review Letters*, *119*(10), 105101. https://doi.org/10.1103/physrevlett.119.105101

Melrose, D. B. (1980). The emission mechanisms for solar radio bursts. *Space Science Reviews*, *26*(1), 3–38. https://doi.org/10.1007/BF00212597

Melrose, D. B. (2017). Coherent emission mechanisms in astrophysical plasmas. *Reviews of Modern Plasma Physics*, *1*(1), 5. https://doi.org/10.1007/s41614-017-0007-0

Morosan, D. E., Carley, E. P., Hayes, L. A., Murray, S. A., Zucca, P., Fallows, R. A., et al. (2019). Multiple regions of shock-accelerated particles during a solar coronal mass ejection. *Nature Astronomy*, *3*(5), 452–461. https://doi.org/10.1038/s41550-019-0689-z

Pulupa, M. P., Bale, S. D., & Kasper, J. C. (2010). Langmuir waves upstream of interplanetary shocks: Dependence on shock and plasma parameters. *Journal of Geophysical Research*, *115*(A4). https://doi.org/10.1029/2009JA014680

Russell, C. T., Hoppe, M. M., & Livesey, W. A. (1982). Overshoots in planetary bow shocks. *Nature*, *296*(5852), 45–48. https://doi.org/10.1038/296045a0

Tang, H.-B., Hao, Y.-F., Hu, G.-Y., Lu, Q.-M., Ren, C., Zhang, Y., et al. (2025). Laboratory observation of ion drift acceleration via reflection off laser-produced magnetized collisionless shocks. *Science Advances*, *11*(7), eadn3320. https://doi.org/10.1126/sciadv.adn3320

Trotta, D., & Burgess, D. (2019). Electron acceleration at quasi-perpendicular shocks in sub- and supercritical regimes: 2D and 3D simulations. *Monthly Notices of the Royal Astronomical Society*, *482*(1), 1154–1162. https://doi.org/10.1093/mnras/sty2756

Williams, J. D., Chen, L.-J., Kurth, W. S., Gurnett, D. A., Dougherty, M. K., & Rymer, A. M. (2005). Electrostatic solitary structures associated with the November 10, 2003, interplanetary shock at 8.7 AU. *Geophysical Research Letters*, *32*(17). https://doi.org/10.1029/2005GL023079

Wu, C. S. (1984). A fast fermi process: Energetic electrons accelerated by a nearly perpendicular bow shock. *Journal of Geophysical Research*, *89*(A10), 8857–8862. https://doi.org/10.1029/JA089iA10p08857

Yang, Z., Liu, Y. D., Johlander, A., Parks, G. K., Lavraud, B., Lee, E., et al. (2020). MMS direct observations of kinetic-scale shock self-reformation. *The Astrophysical Journal*, *901*(1), L6. https://doi.org/10.3847/2041-8213/abb3ff